Synthesis and Characterization of (μ-Hydroxo)bis(μ-acetato)diiron(II) and (μ-Oxo)bis(μ-acetato)diiron(III) 1,4,7-Trimethyl-1,4,7-triazacyclononane Complexes as Models for Binuclear Iron Centers in Biology; Properties of the Mixed Valence Diiron(II,III) Species

JudithAnn R. Hartman,[1a] R. Lynn Rardin,[1a] Phalguni Chaudhuri,[1b] Klaus Pohl,[1b] Karl Wieghardt,*[1b] Bernhard Nuber,[1c] Johannes Weiss,[1c] Georgia C. Papaefthymiou,[1d] Richard B. Frankel,[1d] and Stephen J. Lippard*[1a]

Contribution from the Department of Chemistry and the Francis Bitter National Magnet Laboratory, Massachusetts Institute of Technology, Cambridge, Massachusetts 02139, Lehrstuhl für Anorganische Chemie I, Ruhr-Universität, D-4630 Bochum, FRG, and Anorganisch-Chemisches Institut der Universität, D-6900 Heidelberg, FRG.
Received February 23, 1987

Abstract: The binuclear diiron(II) and diiron(III) compounds $[Fe_2(OH)(OAc)_2(Me_3TACN)_2](ClO_4)\cdot H_2O$ and $[Fe_2O(OAc)_2(Me_3TACN)_2](ClO_4)_2\cdot H_2O$ (Me_3TACN = 1,4,7-trimethyl-1,4,7-triazacyclononane) were synthesized and their structures determined by X-ray crystallography. Both complexes have two facially coordinated Me_3TACN ligands capping a bioctahedral structure with two bridging acetate ligands. The remaining bridging ligand is hydroxide in the ferrous complex and oxide in the ferric complex. The structures are thus analogous to the bridged diiron cores of deoxyhemerythrin and azidomethemerythrin, respectively. The major differences between the diiron(II) and diiron(III) structures are the longer metal-ligand bond lengths and Fe···Fe distance, 3.32 (1) Å vs. 3.12 (1) Å, found in the ferrous complex, with little accompanying angular distortion (the Fe-O-Fe angles are 113.2 (1)° and 119.7 (1)°, respectively). The Mössbauer spectra and bulk magnetic properties of these complexes are very similar to those of hemerythrin in the analogous oxidation states, with δ = 1.16 (3) mm/s, ΔE_Q = 2.83 (5) mm/s, and J = -13 (1) cm^{-1} for the diiron(II) complex and δ = 0.47 (3) mm/s, ΔE_Q = 1.50 (5) mm/s, and J = -119 (1) cm^{-1} for the diiron(III) complex. The redox behavior of these diiron complexes has been measured by cyclic voltammetry. Oxidation of the diiron(II) complex yields one anodic peak and two closely spaced cathodic peaks on the return sweep, tentatively assigned to reduction of oxo- and hydroxo-bridged diiron(II,III) species. In the presence of triethylamine, only one, quasireversible wave appears at -0.29 V versus SCE. CV studies of the diiron(III) complex reveal a quasireversible wave at -0.37 V versus SCE. Thus, as in hemerythrin, the mixed-valence species is thermodynamically unstable with respect to disproportionation. Controlled potential coulometry revealed that $[Fe_2O(OAc)_2(Me_3TACN)_2]^{2+}$ takes up one electron. Electron spin resonance studies of the resulting species reveal features at $g < 2.0$ in frozen glasses at 9.6 K which integrate to 65% of the value expected for one unpaired spin. This result, together with reduced hyperfine fields in the magnetic Mössbauer spectrum, is consistent with a mixed-valence diiron(II,III) formulation.

Binuclear iron centers bridged by an oxo group have proved to be a common unit in biological systems.[2] Proteins such as ribonucleotide reductase,[3] methane monooxygenase,[4] hemerythrin (Hr),[5] and purple acid phosphatase[6] are known or thought to contain this kind of binuclear center in the diiron(III), diiron(II), or mixed-valence diiron(II,III) oxidation state. For example, hemerythrin, an oxygen-carrying protein found in marine invertebrates, is postulated to cycle between diiron(II) and diiron(III) oxidation states as illustrated in eq 1, while the active form of purple acid phosphatase, an enzyme found in mammals, involves the mixed-valence diiron(II,III) oxidation states.

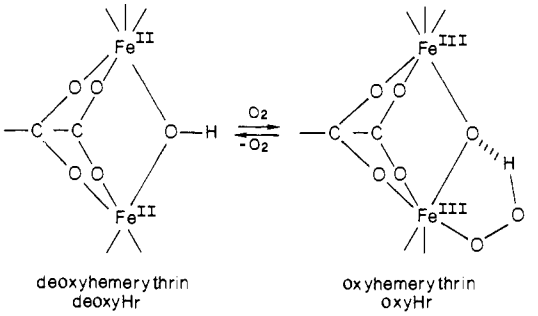

(1)

Although the diiron(III) oxidation level of hemerythrin, the most studied protein of this class, has been well characterized by physical measurements of both the protein[7] and several small molecule model compounds,[8,9] the diiron(II) and mixed-valence oxidation states are less well understood. Complete characterization of the lower oxidation states of hemerythrin has been hampered by the absence of an ESR signal and lack of easily detected optical features for the diiron(II,II) deoxyhemerythrin and by the short lifetime of the mixed-valence, diiron(II,III) semimethemerythrin. In part because of these difficulties, small molecule models can be quite valuable in helping to elucidate the properties of hemerythrin. For example, an important structural feature to be established is whether a hydroxo bridge exists in

(1) (a) Department of Chemistry, MIT. (b) Ruhr-Universität. (c) Universität Heidelberg. (d) Francis Bitter National Magnet Laboratory, MIT.

(2) Lippard, S. J. *Chem. Br.* **1986**, 222-229. Lippard, S. J. *Angew. Chem.*, in press.

(3) (a) Sjöberg, B.-M.; Gräslund, A. *Adv. Inorg. Biochem.* **1983**, *5*, 87-110. (b) Lammers, M.; Follman, H. *Struct. Bonding* **1983**, *54*, 27-91.

(4) Woodland, M. P.; Patil, D. S.; Cammack, R.; Dalton, H. *Biochim. Biophys. Acta* **1986**, *873*, 237-242.

(5) (a) Wilkins, R. G.; Harrington, P. C. *Adv. Inorg. Biochem.* **1983**, *5*, 51-85. (b) Wilkins, P. C.; Wilkins, R. G. *Coord. Chem. Rev.* **1987**, *79*, 195-214.

(6) Antanaitis, B. C.; Aisen, P. *Adv. Inorg. Biochem.* **1983**, *5*, 111-136.

(7) Klotz, I. M.; Kurtz, D. M., Jr. *Acc. Chem. Res.* **1984**, *17*, 16-22.

(8) (a) Armstrong, W. H.; Lippard, S. J. *J. Am. Chem. Soc.* **1983**, *105*, 4837-4838. (b) Armstrong, W. H.; Spool, A.; Papaefthymiou, G. C.; Frankel, R. B.; Lippard, S. J. *J. Am. Chem. Soc.* **1984**, *106*, 3653-3667.

(9) (a) Wieghardt, K.; Pohl, K.; Gebert, W. *Angew. Chem., Int. Ed. Engl.* **1983**, *22*, 727. (b) Chaudhuri, P.; Wieghardt, K.; Nuber, B.; Weiss, J. *Angew. Chem., Int. Ed. Engl.* **1985**, *24*, 778-779. (c) Wieghardt, K.; Pohl, K.; Ventur, D. *Angew. Chem., Int. Ed. Engl.* **1985**, 24, 392-393.

0002-7863/87/1509-7387$01.50/0

deoxyhemerythrin. Several studies have provided indirect evidence for such a group and its involvement in the oxygen-binding reaction (eq 1).[10] The presence or absence of a proton at a specific site in a protein is very difficult to establish by X-ray diffraction methods, and final proof depends upon comparison of observed geometric, spectroscopic and magnetic properties of the protein with those of structurally characterized model compounds.

This paper presents structural and physical studies of the analogous pair of complexes $[Fe_2(OH)(OAc)_2(Me_3TACN)_2](ClO_4)\cdot H_2O$ (**1**) and $[Fe_2O(OAc)_2(Me_3TACN)_2](X)_2$ (X = PF_6 (**2**) or ClO_4 (**3**)), where Me_3TACN = 1,4,7-trimethyl-1,4,7-triazacyclononane, and physical studies of mixed-valence species generated from **1** and **2**. Compound **1** is the first well characterized example of a binuclear iron(II) complex with either a hydroxo or an oxo bridge. Preliminary results were briefly described previously.[9]

Experimental Section

Methods and Materials. The ligand 1,4,7-trimethyl-1,4,7-triazacyclononane was prepared as described previously.[11] All other reagents were purchased from commercial sources and used without further purification. Perchlorate was analyzed gravimetrically as the tetraphenylarsonium salt.

$[Fe_2(OH)(O_2CCH_3)_2(Me_3TACN)_2](ClO_4)\cdot H_2O$ (1). All operations were carried out under anaerobic conditions. Ferrous perchlorate hexahydrate (0.36 g, 1.0 mmol) was added to a stirred solution of 1,4,7-trimethyl-1,4,7-triazacyclononane (0.51 g, 3.0 mmol) in 40 mL of methanol. The resulting solution was stirred at room temperature for 2.5 h to give a deep blue color, which changed immediately to pale yellow upon addition of anhydrous sodium acetate (0.2 g, 2.4 mmol). The reaction mixture was stirred an additional 30 min, after which sodium perchlorate monohydrate (0.4 g, 2.8 mmol) was added and the volume of solution reduced to 15 mL. The resulting greenish-yellow crystals were collected by filtration and recrystallized from methanol. Yield: 150 mg (42%). Anal. Calcd for $Fe_2C_{22}H_{51}N_6O_{10}Cl$: C, 37.38; H, 7.27; N, 11.89; Fe, 15.80; ClO_4, 14.07. Found: C, 37.7; H, 7.1; N, 11.9; Fe, 15.9; ClO_4, 13.9. Optical spectrum (CH_3OH): 928 nm (ϵ 10 cm^{-1} M^{-1}), 1100 nm (sh). IR (KBr, cm^{-1}): 3640 (m), 3420 (m), 2960 (s), 2840 (s), 1620 (s), 1502 (m), 1472 (s), 1424 (s), 1379 (m), 1349 (m), 1313 (m), 1100 (s), 1030 (s), 945 (w), 910 (m), 784 (m), 762 (m), 668 (m), 635 (m), 582 (m). Mass spectrum (FAB): 588 ($M - H^+$), 417 ($M^+ - Me_3TACN$). Calculated molecular weight: 589.4. X-ray quality crystals were obtained by slow evaporation of a methanol solution of **1**.

$[Fe_2O(O_2CCH_3)_2(Me_3TACN)_2](PF_6)_2$ (2). A solution of 1,4,7-trimethyl-1,4,7-triazacyclononane (2.0 g, 11.7 mmol) in 12 mL of absolute ethanol was added dropwise to a stirred solution of ferric chloride hexahydrate (3.5 g, 13.0 mmol) in 100 mL of ethanol. The resulting mustard colored precipitate of $Fe(Me_3TACN)Cl_3$[12] was collected by filtration, washed with ethanol and diethyl ether, and then dried to give 3.7 g (95%) of yellow solid.

A mixture of $Fe(Me_3TACN)Cl_3$ (3.0 g, 9.0 mmol) and sodium acetate (2.0 g, 24 mmol) in 150 mL of absolute ethanol was stirred at room temperature for 2 h and then filtered to remove precipitated sodium chloride. Ammonium hexafluorophosphate (3.0 g, 18 mmol) was added and the reddish-brown solution was cooled to 0 °C. The resulting reddish-brown solid was collected by filtration and recrystallized from methanol to give 2.56 g (65%) of product as brown needles. Anal. Calcd for $Fe_2C_{22}H_{48}N_6O_5P_2F_{12}$: C, 30.09; H, 5.51; N, 9.57; P, 7.05; Fe, 12.7. Found: C, 30.0; H, 5.5; N, 9.6; P, 7.1; Fe, 13.0. UV-vis (H_2O): 345 nm (ϵ = 10500 cm^{-1} mol^{-1} L), 428 (1000), 475 (1560), 519 (1200), 550 (sh), 734 (120). IR (KBr, cm^{-1}): 3600 (w), 2980 (m), 2900 (m), 1553 (s), 1498 (m), 1467 (s), 1384 (w), 1368 (w), 1357 (w), 1305 (m), 1167 (m), 1136 (w), 1082 (m), 1078 (m), 1017 (s), 997 (m), 847 (s), 794 (m), 757 (m), 729 (s), 671 (m), 578 (m). Mass spectrum (FAB): 589 (M^+). Calculated molecular weight: 588.4.

$[Fe_2O(O_2CCH_3)_2(Me_3TACN)_2](ClO_4)_2\cdot H_2O$ (3). Air oxidation of a methanolic solution of **1** led to a deep red-brown solution. Evaporation of this solution from an open vessel yielded X-ray quality red-brown dichroic crystals after 48 h. Anal. Calcd for $Fe_2C_{22}N_6O_{14}Cl_2$: C, 32.81; H, 6.26; N, 10.44; ClO_4, 24.70. Found: C, 32.6; H, 6.1; N, 10.2; ClO_4, 24.9. UV-vis (CH_3OH): 1031 nm (ϵ = 7 cm^{-1} mol^{-1} L), 729 (143), 549 (sh), 513 (1100), 472 (1450), 424 (960). IR (KBr, cm^{-1}, selected peaks): 1540 (vs), 1460 (vs), 1442 (vs), 710 (m).

Table I. Experimental Details of X-ray Diffraction Studies of $[Fe_2(OH)(O_2CCH_3)_2(Me_3TACN)_2](ClO_4)\cdot H_2O$ (**1**) and $[Fe_2O(O_2CCH_3)_2(Me_3TACN)_2](ClO_4)_2\cdot H_2O$ (**3**)

	1	**3**
(A) Crystal Parameters[a,b]		
a, Å	10.92 (1)	13.078 (2)
b, Å		17.732 (3)
c, Å	27.85 (3)	15.290 (3)
crystal system	tetragonal	orthorhombic
space group	$P4_12_12$ (D_4^4)	$Amam$ (D_{2h}^{17})
Z	4	4
V, Å^3	3321	3545.7
ρ_{calcd}, g cm^{-3}	1.416	1.513
mol wt	706.82	805.26
(B) Measurement and Treatment of Intensity Data		
instrument	AED II (Siemens)	Syntex R2
radiation	Mo Kα (λ = 0.710 73 Å), graphite monochromatized	
scan type	ω	θ–2θ
2θ limits, deg	62	60
no. of reflcns collcd	1278	3024
no. of reflcns ($I > 1.5\sigma(I)$)	1264	2980
abs cor[c]		
cryst size	1.0 × 1.0 × 0.2 mm	0.3 × 0.4 × 0.5 mm
linear abs coeff, cm^{-1}	9.47	9.69
transmission factors	0.51–0.72	0.47–0.58
(C) Final Model in Least-Squares Refinement		
final R values[d]		
R_1	0.082	0.079
R_2	0.069	0.078
no. of variable params	184	117

[a] From a least-squares fit to the setting angles of 25 reflections with $2\theta \geq 20°$. [b] Unit cell parameters and data collection at 22 ± 1 °C. [c] Empirical absorption corrections (ψ-scans). [d] $R_1 = \sum||F_o| - |F_c||/\sum|F_o|$; $R_2 = [\sum w(|F_o|^2 - |F_c|^2)/\sum w|F_o|^2]^{1/2}$, $w = 1/\sigma^2(I)$.

Collection and Reduction of X-ray Data. $[Fe_2(OH)(O_2CCH_3)_2(Me_3TACN)_2](ClO_4)\cdot H_2O$. A yellow, tabular-shaped crystal of **1** was coated with a thin film of polyester glue and attached to a glass fiber. The crystal quality was found to be acceptable on the basis of ω-scans of several low-angle reflections ($\overline{\Delta\omega_{1/2}} = 0.3°$). The crystal was determined to have one of the enantiomorphic pair of polar tetragonal space groups $P4_12_12$ (D_4^4, No. 92) or $P4_32_12$ (D_4^8, No. 96)[13] from the systematic absences $h00$, $h \neq 2n$ and $00l$, $l \neq 4n$. Further details of the data collection and reduction are given in Table I.

$[Fe_2O(O_2CCH_3)_2(Me_3TACN)_2](ClO_4)_2\cdot H_2O$. A dichroic reddish-brown/green, block-shaped crystal of **3** was mounted on a glass fiber with polyester glue. Several ω-scans of low-angle reflections with 0.3° half-widths showed the crystal to be of acceptable X-ray quality. Compound **3** was found to crystallize in the orthorhombic system, with possible space groups $Amam$ (D_{2h}^{17}, No. 63 in a non-standard setting), $A2_1am$ (C_{2v}^{12}, No. 36 in a non-standard setting), or $Ama2$ (C_{2v}^{16}, No. 40),[14] based on the systematic absences hkl, $k + l \neq 2n$; $h0l$, $h \neq 2n$. Crystal parameters and additional details of the data collection and reduction are given in Table I.

Structure Solution and Refinement. Both structures were solved by standard Patterson and difference Fourier methods and refined with anisotropic thermal parameters for all non-hydrogen atoms, with the exception of oxygen atoms of disordered perchlorate anions, which were refined isotropically in both structures. Neutral atom scattering factors and anomalous dispersion corrections for non-hydrogen atoms were taken from ref 15 and hydrogen atom scattering factors from ref 16. All methylene hydrogen atoms were placed at calculated positions with d(C–H) = 0.96 Å, while the methyl groups were treated as rigid bodies, each with three rotational variables. The function minimized during refinement was $\sum w(|F_o| - |F_c|)^2$, where $w = 1/\sigma^2(F_o^2)$. The choice of

(10) (a) Shiemke, A. K.; Loehr, T. M.; Sanders-Loehr, J. *J. Am. Chem. Soc.* **1986**, *108*, 2437–2443. (b) Maroney, M. J.; Kurtz, D. M., Jr.; Nocek, J. M.; Pearce, L. L.; Que, L., Jr. *J. Am. Chem. Soc.* **1986**, *108*, 6871–6879.
(11) Wieghardt, K.; Chaudhuri, P.; Nuber, B.; Weiss, J. *Inorg. Chem.* **1982**, *21*, 3086–3090.
(12) Wieghardt, K.; Pohl, K.; Ventur, D. *Angew. Chem., Int. Ed. Engl.* **1985**, *24*, 392–393.
(13) Hahn, T., Ed. *International Tables for Crystallography*; D. Reidel: Dordrecht, Holland, 1983; Volume A, pp 358 and 366.
(14) Hahn, T., Ed. *International Tables for Crystallography*; D. Reidel: Dordrecht, Holland, 1983; Volume A, pp 230, 238, and 290.
(15) *International Tables of Crystallography*; Kynoch: Birmingham, England, 1974; Vol. IV, pp 99 and 149.
(16) Stewart, R. F.; Davidson, E. R.; Simpson, W. T. *J. Chem. Phys.* **1965**, *42*, 3175–3187.

Table II. Atomic Coordinates for $[Fe_2(OH)(O_2CCH_3)_2(Me_3TACN)_2](ClO_4)\cdot H_2O$ (**1**)[a,b]

atom	*x*	*y*	*z*
Fe	0.4928 (2)	0.3302 (2)	0.2163 (1)
Cl	0.4371 (5)	0.4371 (5)	0.5000
O1	0.6522 (8)	0.3478 (8)	0.2500
O2	0.4718 (9)	0.5164 (8)	0.1935 (3)
O3	0.3828 (9)	0.3579 (8)	0.2781 (3)
N1	0.5673 (9)	0.2624 (11)	0.1455 (4)
N2	0.3197 (10)	0.2995 (10)	0.1709 (4)
N3	0.475 (1)	0.120 (1)	0.2220 (4)
C1	0.542 (1)	0.062 (1)	0.1822 (6)
C2	0.625 (1)	0.158 (1)	0.1569 (7)
C3	0.485 (2)	0.259 (2)	0.1098 (6)
C4	0.350 (1)	0.326 (1)	0.1226 (5)
C5	0.283 (1)	0.162 (2)	0.1772 (6)
C6	0.332 (2)	0.105 (1)	0.2200 (6)
C7	0.518 (1)	0.705 (1)	0.1583 (5)
C8	0.546 (1)	0.598 (1)	0.1933 (5)
C11	0.664 (2)	0.365 (2)	0.1274 (5)
C12	0.217 (2)	0.375 (2)	0.1875 (5)
C13	0.919 (1)	0.484 (2)	0.2316 (6)
O11	0.525 (3)	0.341 (3)	0.4834 (9)
O12	0.513 (5)	0.477 (5)	0.537 (2)
O13	0.524 (5)	0.524 (5)	0.5000
O14	0.328 (4)	0.359 (4)	0.481 (1)
O15	0.387 (6)	0.437 (6)	0.457 (2)
O_W	0.238 (2)	0.238 (2)	0.0000

[a] For atom labels, see Figure 2. [b] Numbers in parentheses are estimated standard deviations in the last digit.

Table III. Atomic Coordinates for $[Fe_2O(O_2CCH_3)_2(Me_3TACN)_2](ClO_4)_2\cdot H_2O$ (**3**)[a,b]

atom	*x*	*y*	*z*
Fe	0.25000	0.19241 (5)	0.39820 (6)
Cl1	0.25000	0.5120 (2)	0.50000
Cl2	0.25000	0.3725 (2)	0.0000
O1	0.25000	0.1415 (3)	0.5000
O2	0.1340 (3)	0.2645 (2)	0.4274 (2)
N1	0.3582 (3)	0.1223 (2)	0.3241 (2)
N2	0.2500	0.2517 (3)	0.2668 (4)
C1	0.3944 (6)	0.1636 (4)	0.2466 (5)
C2	0.3427 (6)	0.2289 (4)	0.2207 (5)
C3	0.3042 (5)	0.0526 (3)	0.2988 (6)
C5	0.0980 (5)	0.2825 (4)	0.5000
C6	0.0047 (7)	0.3273 (5)	0.5000
C7	0.4472 (5)	0.1012 (4)	0.3766 (4)
C8	0.2500	0.3343 (4)	0.2803 (6)
O_W	0.0000	0.0000	0.1504 (6)
O11	0.2500	0.5825 (22)	0.5000
O12	0.310 (1)	0.5281 (9)	0.572 (1)
O21	0.193 (1)	0.4033 (7)	0.071 (1)
O22	0.168 (4)	0.436 (2)	0.000
O13	0.154 (2)	0.476 (2)	0.5000
O23	0.2500	0.304 (2)	0.0000

[a] For atom labels, see Figure 1. [b] See footnote *b*, Table II.

polarity for complex **1** was confirmed by refinement of the data in both settings. The largest ratio of parameter shift to estimated standard deviation in the final cycle of refinement was 0.2 in both cases for all atoms except the disordered perchlorate oxygen atoms. Final positional parameters are presented in Tables II and III, while interatomic distances and angles are given in Tables IV and V. Observed and calculated structure factors are given in Tables S1 and S2, and final thermal parameters for all non-hydrogen atoms are supplied in Tables S3 and S4. Final positional and thermal parameters for the hydrogen atoms are given in Tables S5 and S6.

Physical Measurements. Electrochemistry. Electrochemical experiments were performed with a Princeton Applied Research (PAR) Model 173 potentiostat, a PAR Model 175 universal programmer, a Model 179 digital coulometer, and a Houston Instruments Model 2000 X–Y plotter. Electrochemical measurements were made on methylene chloride solutions containing 0.2 M tetra-*n*-butylammonium tetrafluoroborate (TBAT) as supporting electrolyte, unless otherwise stated, and were conducted at room temperature under a nitrogen atmosphere. A standard three-electrode system was used for cyclic voltammetry (CV) experiments comprising a glassy carbon working electrode, a platinum

Table IV. Bond Distances (Å) for $[Fe_2O(O_2CCH_3)_2(Me_3TACN)_2](ClO_4)_2\cdot H_2O$ (**3**) and $[Fe_2(OH)(O_2CCH_3)_2(Me_3TACN)_2](ClO_4)\cdot H_2O$ (**1**)[a]

	3	**1**
Fe–O1	1.800 (3)	1.987 (8)
Fe–O2	2.034 (3)	2.142 (9)
Fe–O3		2.12 (1)
Fe–N1	2.198 (4)	2.26 (1)
Fe–N2	2.268 (6)	2.30 (1)
Fe–N3		2.31 (1)
Fe···Fe	3.12 (4)	3.32 (1)
C1–C2	1.398 (9)	1.55 (2)
C3–C3A	1.418 (9)	
C3–C4		1.69 (3)
C5–C6	1.456 (10)	1.44 (2)
C7–C8		1.55 (2)
O2–C5	1.246 (4)	
O2–C8		1.20 (2)
O3–C8A		1.34 (2)
N1–C1	1.472 (7)	
N1–C2		1.34 (2)
N1–C3	1.475 (7)	1.34 (2)
N1–C7	1.462 (7)	1.62 (2)
N2–C2	1.459 (7)	
N2–C4		1.42 (2)
N2–C5		1.56 (2)
N2–C8	1.480 (10)	1.47 (2)
N3–C1		1.48 (2)
N3–C6		1.57 (2)
N3–C13		1.43 (2)

[a] See Figures 1 and 2 for atom labeling scheme. Numbers in parentheses are standard deviations in the last digit(s) listed.

Table V. Bond Angles (deg) for $[Fe_2O(O_2CCH_3)_2(Me_3TACN)_2](ClO_4)_2\cdot H_2O$ (**3**) and $[Fe_2(OH)(O_2CCH_3)_2(Me_3TACN)_2](ClO_4)\cdot H_2O$ (**1**)[a]

		3	
O1–Fe–O2	97.2 (2)	O1–Fe–N1	99.3 (2)
O1–Fe–N2	176.9 (5)	O2–Fe–N1	161.7 (8)
O2–Fe–N2	84.4 (2)	Fe–O1–FeB	119.7 (1)
N1–Fe–N1A	80.2 (2)	Fe–O2–C5	129.6 (5)
O1–Fe–O2A	97.2 (3)	O2–C5–C6	117.2 (6)
O2–Fe–O2A	96.5 (2)	O2–C5–O2AB	125.9 (5)
O2A–Fe–N1	89.4 (2)	Fe–N1–C1	109.9 (4)
N1–Fe–N2	78.8 (2)	C1–N1–C7	108.2 (6)
Fe–N2–C2	107.4 (3)	Fe–N1–C3	107.5 (3)
C2–N2–C8	110.0 (6)	Fe–N1–C7	112.0 (3)
Fe–N2–C8	109.6 (4)	C1–N1–C3	111.1 (6)
C2–N2–C2A	112.3 (7)	C3–N1–C7	108.1 (6)
N1–C1–C2	119.0 (6)	N1–C3–C3A	118.6 (6)
N2–C2–C1	119.6 (6)		
		1	
O1–Fe–O2	98.2 (4)	Fe–O1–FeA	113.2 (2)
O1–Fe–O3	95.6 (5)	Fe–O2–C8	129.2 (8)
O2–Fe–O3	92.6 (5)	Fe–N1–C2	104.0 (8)
N2–Fe–N3	79.8 (5)	C2–N1–C11	110.8 (8)
O1–Fe–N1	97.4 (4)	Fe–N2–C4	107.5 (8)
O2–Fe–N1	95.3 (6)	C4–N2–C12	111.1 (8)
N1–Fe–N2	76.6 (5)	Fe–N3–C1	109.5 (9)
N2–Fe–O3	90.1 (5)	C1–N3–C13	113.1 (9)
O1–Fe–N2	174.2 (7)	Fe–N1–C3	114.5 (10)
O2–Fe–N2	83.6 (5)	C3–N1–C11	102.9 (12)
N1–Fe–N3	76.4 (6)	Fe–N2–C5	106.9 (8)
N3–Fe–O3	92.2 (5)	C5–N2–C12	107.9 (12)
O1–Fe–N3	97.9 (7)	Fe–N3–C6	100.5 (7)
O2–Fe–N3	162.8 (3)	C6–N3–C13	108.2 (10)
N1–Fe–O3	163.9 (3)	Fe–N1–C11	106.2 (8)
N3–C1–C2	109.9 (10)	Fe–N2–C12	112.0 (10)
Fe–O3–C8	120.5 (10)	Fe–N3–C13	109.5 (10)
O2–C8–O3A	130.1 (13)	C2–N1–C3	117.8 (15)
N1–C2–C1	114.1 (15)	C4–N2–C5	111.4 (15)
N2–C4–C3	108.2 (13)	C1–N3–C6	115.2 (17)
N3–C6–C5	110.7 (13)	O2–C8–C7	115.4 (11)
N2–C5–C6	114.0 (13)	O3A–C8–C7	114.1 (11)
N1–C3–C4	114.8 (11)		

[a] See Figures 1 and 2 for atom labeling scheme. Numbers in parentheses are estimated standard deviations in the last digit(s) listed.

auxiliary electrode, and a PAR saturated calomel electrode separated from the bulk solution by a bridge containing TBAT in methylene chloride. Vycor plugs were used at all solution junctions. The performance of the reference electrode was monitored by measuring the Fe(0/+) couple of ferrocene, which was found to have a value of +0.47 V. Controlled potential coulometry (CPC) experiments were carried out with use of the same apparatus, with the substitution of a platinum gauze basket for the working electrode and a platinum coil for the auxiliary electrode.

Mössbauer Spectroscopy. Mössbauer spectra were recorded with a conventional constant acceleration spectrometer equipped with a temperature controller, maintaining temperatures within ±0.1 K, and an Nb_3Ti superconducting magnet, producing fields up to 80 kOe, parallel to the direction of the γ-rays. The source used was ^{57}Co in Rh, and the isomer shifts were referenced to metallic iron at room temperature.

Mass Spectra. Mass spectra were recorded with a Finnigan MAT System 8200 mass spectrometer.

Electron Spin Resonance (ESR) Spectroscopy. ESR spectra were recorded with a Varian E9 spectrometer with diphenylpicrylhydrazyl as calibrant (g = 2.0037). Cylindrical 3-mm quartz tubes were used for both powder and frozen glass samples.

Optical and Infrared Spectroscopy. Electronic absorption spectra in the 300–1200-nm range were recorded with a Perkin-Elmer LAMBDA 9 spectrophotometer, while infrared spectra were recorded with a Perkin-Elmer Model 283B spectrometer.

Magnetic Susceptibility Measurements. Solid-state magnetic susceptibilities for 26.0 mg of powdered **1** and 42.9 mg of powdered **2** were measured at 10 kG, using a SHE Model 905 SQUID-type susceptometer. A total of 43 data points for **1** and 54 data points for **2** were taken over the temperature range 6.0–300 K. The susceptibilities of the Si–Al alloy sample holder used in the experiment were measured at the same temperature points to allow for correction of the paramagnetic contribution of the sample holder to the total susceptibility. Pascal's constants[17,18] were used to calculate the diamagnetic correction of −408 emu G^{-1} mol^{-1} for **1** and −485 emu G^{-1} mol^{-1} for **2**. The theoretical expression (vide infra) was fit to the data by a non-linear least-squares method by using a locally written program.[19] The absence of ferromagnetic impurities in both compounds was confirmed by measurements of susceptibility in fields ranging from 0.5 to 50 kG at temperatures of 75, 150, and 300 K. No field dependence was observed in either compound.

Results and Discussion

Synthesis. In the last 5 years, the interest in proteins having binuclear iron functional centers has greatly increased,[2] a trend that has been paralleled by an increase in the number of synthetic binuclear iron model compounds.[8,9,20,21] The majority of these complexes are comprised of a diiron(III) core with two bridging carboxylate groups and a bridging oxo group. Furthermore, the observation that this diiron(III) core readily assembles with a variety of tridentate, nitrogen-containing, capping ligands suggests that it is a particularly stable configuration. Indeed, this hypothesis is supported by the wide variety of synthetic routes used to generate complexes of this type. For example, the $[Fe_2O(OAc)_2(Me_3TACN)_2]^{2+}$ (vide supra) and $[Fe_2O(OAc)_2(TACN)_2]^{2+}$[9a] cations are prepared by combining $Fe(TACN)Cl_3$ monomers with acetate ions; $[Fe_2O(OAc)_2(HBpz_3)_2]$ is formed by mixing ferric perchlorate, sodium acetate, and hydrotris(pyrazolyl)borate in a single reaction vessel;[8] $[Fe_2O(O_2CPh)_2(HBpz_3)_2]$ is prepared by adding sodium benzoate to a preformed μ-oxo binuclear complex, $[Fe_2OCl_6]^{2-}$, followed by addition of $K(HBpz_3)$;[8] and $[Fe_2O(OAc)_2(TBPN)]_2^{4+}$ is formed by addition of the TBPN ligand to the basic ferric acetate cluster.[21] It is therefore not surprising that this type of diiron(III) core is also known or believed to occur in nature in a wide variety of proteins, including oxygenases, phosphatases, and oxygen carriers.[2]

In contrast to the many recent reports of binuclear ferric complexes, no (μ-hydroxo)bis(μ-carboxylato)diiron(II) complex had been prepared before the present work. Since the binuclear iron core in the protein hemerythrin exists in both ferrous and ferric oxidation states,[7] one might have expected that the diiron(II) core would self-assemble in model complexes, given a judicious choice of starting materials. Indeed, $[Fe_2(OH)(OAc)_2(Me_3TACN)_2](ClO_4)\cdot H_2O$ readily crystallizes from a mixture of sodium acetate, ferrous perchlorate, and Me_3TACN. The Me_3TACN ligand was chosen because it is a facially coordinating tridentate nitrogen ligand that is apparently too bulky to form $[Fe(Me_3TACN)_2]^{2+}$, a species expected to be the major side-product encountered during attempts to synthesize the desired diiron(II) center.[8]

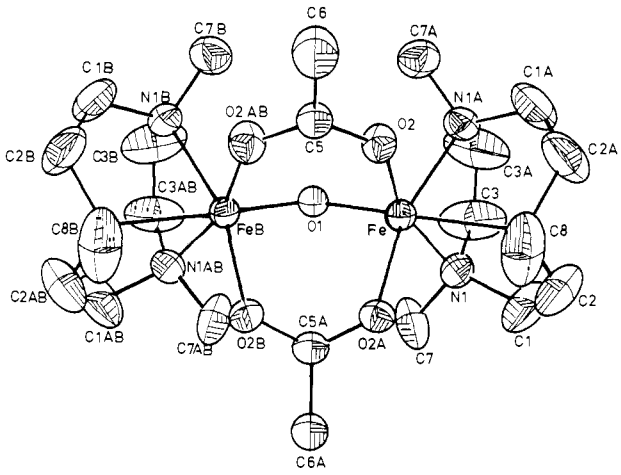

Figure 1. Structure of the $[Fe_2O(O_2CCH_3)_2(Me_3TACN)_2]^{2+}$ cation in **3**, showing 40% probability thermal ellipsoids and the atom labeling scheme.

In previous work, it was demonstrated[8,20] that spontaneous self-assembly of binuclear ferric complexes from ferric perchlorate, sodium acetate, and potassium hydrotris(1-pyrazolyl)borate results in a mixture of hydroxo- and oxo-bridged diiron(III) complexes. Since the reaction was carried out at ca. pH 3.5, the pK_a of the bridging oxo group was estimated to be ~3.5.[2] For the hydrotris(1-pyrazolyl)borate binuclear ferric system, the oxo-bridged species appears to be more stable under the reaction conditions, since longer reaction times result in less hydroxo-bridged and more oxo-bridged product.[20] Similarly, the oxo-bridged $[Fe_2O(OAc)_2(Me_3TACN)_2]^{2+}$ cation appears to be more stable than the analogous hydroxo-bridged complex, since no hydroxo-bridged species was isolated in our reactions. In contrast, spontaneous self-assembly of the binuclear ferrous complex from ferrous perchlorate, sodium acetate, and Me_3TACN results in a hydroxo-bridged species, with no apparent formation of the analogous oxo-bridged compound. A detailed study of the pK_a values of the hydroxo bridges in these and related complexes would be interesting, since the observed behavior appears to mirror that of hemerythrin (Hr), which is proposed to have an oxo bridge in the diiron(III) methemerythrin form and a hydroxo bridge in diiron(II) deoxyhemerythrin.[7,26,27,31,32] The degree of protonation of the bridging oxygen atom has been invoked to rationalize differences in magnetic behavior in various ligand adducts of deoxyHr.[31] The type of bridge that occurs in the mixed-valence, semi-met form of Hr is presently uncertain, although recent evidence favors a hydroxo bridge.[10b]

Description of Structures. The Diiron(III) Complex. The $[Fe_2O(OAc)_2(Me_3TACN)_2](ClO_4)_2\cdot H_2O$ complex has crystallographically required *mm* site symmetry. Each iron atom has a distorted octahedral coordination sphere comprised of two bridging carboxylates, a bridging oxo group, and a facially coordinating tridentate nitrogen ligand (Figure 1). The structure is thus quite similar to that reported previously for $[Fe_2O(OAc)_2(TACN)_2]^{2+}$.[9a,22] The largest deviation from idealized 90° interbond angles is 11.2° and occurs within the five-membered

(17) Carlin, R. L. In *Magnetochemistry*; Springer-Verlag: New York, 1986; p 3.
(18) O'Connor, C. J. *Prog. Inorg. Chem.* **1982**, *29*, 203–283.
(19) Karlin, K., Ph.D. Dissertation, Columbia University, 1975.
(20) Armstrong, W. H.; Lippard, S. J. *J. Am. Chem. Soc.* **1984**, *106*, 4632–4633.
(21) Toftlund, H.; Murray, K. S.; Zwack, P. R.; Taylor, L. F.; Anderson, O. P. *J. Chem. Soc., Chem. Commun.* **1986**, 191–193. TBPN = (*N,N,N',N'*-tetrakis(2-pyridylmethyl)-1,3-propanediamine.
(22) Spool, A.; Williams, I. D.; Lippard, S. J. *Inorg. Chem.* **1985**, *24*, 2156–2162.

N–Fe–N chelate ring. The Fe–N bond lengths (average 2.221 (6) Å) are larger than those found in the analogous complex formed from the unalkylated triazacrown TACN (average 2.18 (1) Å).[9a,22] Similar increases of M–N bond lengths upon alkylation of secondary amines have been observed in a series of Cu(II) complexes of *N*-methyl- and *N*-ethyl-substituted ethylenediamines.[23] The longest Fe–N bond in **3** is the one trans to the bridging oxo group (Table IV). The structural trans influence of this ligand has been well established,[8,9a,22] but the 0.07-Å difference in Fe–N bond lengths cis and trans to the μ-oxo ligand observed in **3** is the largest yet found in binuclear diiron(III) complexes.

Although the C–N bond lengths found in the Me_3TACN ligand are unremarkable (range, 1.459 (7)–1.480 (10) Å), the C–C bond lengths are short (range, 1.398 (9)–1.456 (10) Å) compared to the normal value of 1.54 Å. Such short C–C bond lengths are often observed in crown complexes,[24] primarily due to uncorrected thermal motion. The large thermal parameters observed for the carbon atoms in the present compounds support this explanation.

The bond lengths and angles found in the bridging (μ-oxo)-bis(μ-acetato)diiron(III) core of **3** are generally within the range of those found in published diiron(III) compounds. The Fe···Fe distance of 3.12 (1) Å observed in the Me_3TACN complex, however, is larger than that in the TACN analogue, 3.063 (5) Å,[9a,22] although comparable to the values reported for other (μ-oxo)bis(μ-acetato)diiron(III) compounds, 3.1457 (6) Å in $[Fe_2O(OAc)_2(HBpz_3)_2]$[8] and 3.129 (2) Å in $[Fe_2O(OAc)_2(TBPN)]_2^{4+}$.[21] The anomalously small Fe···Fe distance found in the TACN diiron(III) complex is probably caused by the reduced interligand van der Waals repulsions found with this relatively small, highly constrained ligand.[25] The Fe–O–Fe angle of 119.7 (1) Å in the Me_3TACN complex is very close to the angles measured in all of the other model compounds, 118.7 (4)° and 118.3 (5)° in the TACN complex,[9a,22] 123.6 (1)° in the hydrotris(pyrazolyl)borate complex,[8] and 121.3 (3)° in the TBPN compound.[21]

The iron–iron distances observed in all of these compounds are slightly smaller than the value of 3.25 Å measured for azidomethemerythrin by X-ray crystallography[26] and much shorter than the iron–iron distances of 3.49 Å[27] and 3.38 Å[28] measured by EXAFS. The Fe–O–Fe angles found in these model compounds are also somewhat smaller than the values of 135° and 152° measured in azidomethemerythrin by X-ray diffraction[26] and EXAFS,[27] respectively. The discrepancy between these X-ray diffraction and EXAFS values is most probably due to a failure to fit adequately the second shell in the EXAFS experiment. Reexamination of the EXAFS data including second shell contributions has determined an Fe···Fe distance of 3.20 Å,[29] a value much closer to the Fe···Fe distance determined by X-ray crystallography for both azidomethemerythrin and the model compounds.

The Diiron(II) Complex. The structure of the binuclear ferrous complex, $[Fe_2(OH)(OAc)_2(Me_3TACN)_2](ClO_4)\cdot H_2O$ (**1**), consists of two octahedral iron atoms bridged by one hydroxo group and two acetate groups. The pseudooctahedral coordination spheres are completed by facially coordinating, tridentate Me_3TACN ligands which distort the coordination geometry angles about each iron atom. The greatest deviation from an ideal 90° angle is 13.4°, occurring in the N–Fe–N chelate ring. The structure is shown in Figure 2.

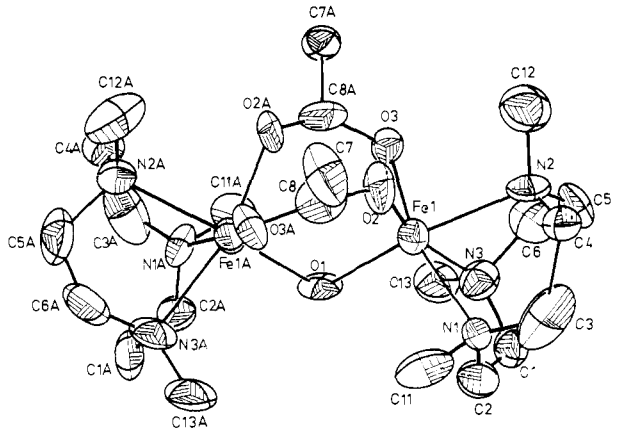

Figure 2. Structure of the $[Fe_2(OH)(O_2CCH_3)_2(Me_3TACN)_2]^+$ cation in **1**, showing 40% probability thermal ellipsoids and the atom labeling scheme.

Large deviations from normal bond lengths are observed in the Me_3TACN ligand, with C–C bonds ranging from 1.44 (2) to 1.69 (3) Å and C–N bonds ranging from 1.34 (2) to 1.57 (2) Å. The scatter observed in these values may in part reflect disorder of the perchlorate anion in the crystal.

The structure of **1** is very similar to that of **3**, but with longer Fe–O and Fe–N bond lengths, average values being 2.090 (9) Å for Fe–O and 2.29 (1) Å for Fe–N in **1** and 1.956 (3) Å for Fe–O and 2.221 (6) Å for Fe–N in **3**; a longer Fe···Fe distance, 3.32 (1) Å in **1** and 3.12 (1) Å in **3**; and a smaller Fe–O–Fe angle in the diiron(II) complex, 113.2 (2)° in **1** versus 119.7 (1)° in **3**. The Fe–N and Fe–O bond lengths in **1** are consistent with a d^6 high-spin electronic configuration, in which the covalent radius of iron is larger than in a high-spin d^5 ion. The Shannon covalent radii are 0.92 and 0.78 Å, respectively,[30] a difference that probably contributes to the larger Fe···Fe distance and smaller Fe–O–Fe angle. In addition, protonation of the μ-oxo bridge without a change in oxidation state would lengthen the Fe···Fe distance, although it would not necessarily change the Fe–O–Fe angle. For example, $[Fe_2O(OAc)_2(HBpz_3)_2]$ has an Fe···Fe distance of 3.1457 (6) Å and an Fe–O–Fe angle of 123.6 (1)°,[8] while $[Fe_2(OH)(OAc)_2(HBpz_3)_2]^+$ has an Fe···Fe distance of 3.439 (1) Å and an Fe–O–Fe angle of 123.1 (2)°.[20] Differences in the bridged diiron core between **1** and **3** are thus a result of both the change in oxidation state and the protonation of the μ-oxo group. Since no other hydroxo-bridged or oxo-bridged diiron(II) complexes have been structurally characterized, the relative contributions to the core structure of protonating the oxo bridge and reducing the iron atoms cannot be assessed. In contrast to **3**, no lengthening of the Fe–N bond trans to the μ-oxo group was observed in **1**. The failure of a μ-OH group to exert a structural trans effect was previously observed for the binuclear ferric analogue.[20]

The geometry of $[Fe_2(OH)(OAc)_2(Me_3TACN)_2](ClO_4)\cdot H_2O$ supports the structure proposed for deoxyhemerythrin on the basis of MCD and ESR[31] and X-ray diffraction[32] measurements but differs from the model proposed on the basis of EXAFS studies.[33] Although both proposed models incorporate two bridging carboxylate residues, the MCD–ESR and X-ray model has a bridging hydroxo group, whereas the model based on EXAFS has a monodentate hydroxo group. The Fe···Fe distance of 3.32 (1) Å found in $[Fe_2(OH)(OAc)_2(Me_3TACN)_2]^+$ is longer than the Fe···Fe distance of 3.13 (3) Å measured in deoxyhemerythrin by EXAFS.[33] Although the published X-ray diffraction results on deoxyhemerythrin[32] were of too low a resolution to give an Fe···Fe distance, difference electron density maps indicated the distance

(23) Pajunen, A.; Luukonen, E. *Suom Kemistil. B* **1969**, *42B*, 348–353.
(24) Dalley, N. K. In *Synthetic Multidentate Macrocyclic Compounds*; Academic: New York, 1978; pp 207–243.
(25) Thom, V. J.; Boeyens, J. C. A.; McDougall, G. J.; Hancock, R. D. *J. Am. Chem. Soc.* **1984**, *106*, 3198–3207.
(26) Stenkamp, R. E.; Sieker, L. C.; Jensen, L. H. *J. Am. Chem. Soc.* **1984**, *106*, 618–622.
(27) Elam, W. T.; Stearn, E. A.; McCallum, J. D.; Sanders-Loehr, J. *J. Am. Chem. Soc.* **1982**, *104*, 6369–6373.
(28) Hendrickson, W. A.; Co, M. S.; Smith, J. L.; Hodgson, K. O.; Klippenstein, G. L. *PNAS, USA* **1982**, *79*, 6255–6259.
(29) Hedman, B.; Co, M. S.; Armstrong, W. H.; Hodgson, K. O.; Lippard, S. J. *Inorg. Chem.* **1986**, *25*, 3708–3711.
(30) Shannon, R. D. *Acta Crystallogr.* **1976**, *A32*, 751–767.
(31) (a) Reem, R. C.; Solomon, E. I. *J. Am. Chem. Soc.* **1984**, *106*, 8323–8325. (b) Reem, R. C.; Solomon, E. I. *J. Am. Chem. Soc.* **1987**, *109*, 1216–1226.
(32) Stenkamp, R. E.; Sieker, L. C.; Jensen, L. H.; McCallum, J. D. *Proc. Natl. Acad. Sci., USA* **1985**, *82*, 713–716.
(33) Elam, W. T.; Stern, E. A.; McCallum, J. D.; Sanders-Loehr, J. *J. Am. Chem. Soc.* **1983**, *105*, 1919–1923.

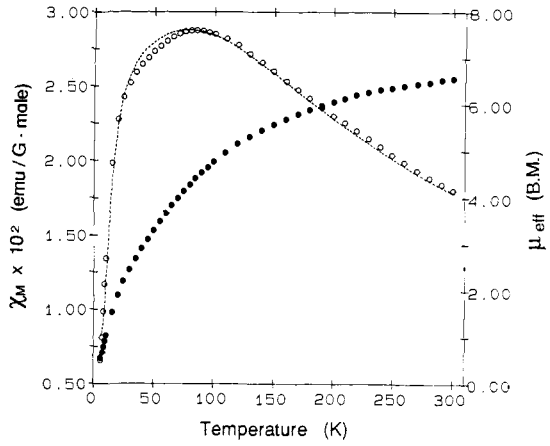

Figure 3. Plots of χ_M (○) and μ_{eff} (●) vs T for solid **1**. The dashed line represents the best least-squares fit of eq 2 (see text) to the experimental susceptibility data.

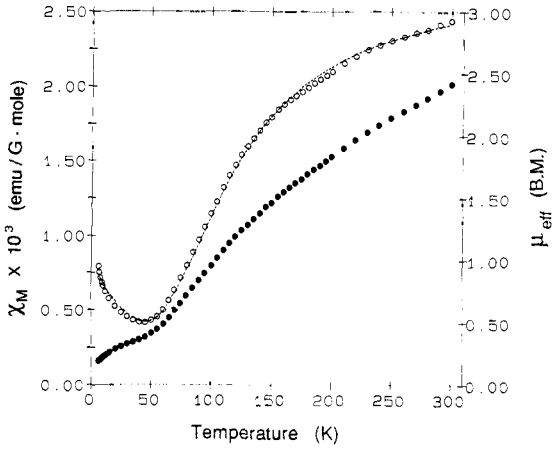

Figure 4. Plots of χ_M (○) and μ_{eff} (●) vs T for solid **2**. The dashed line represents the best least-squares fit of eq 3 (see text) to the experimental susceptibility data.

to be larger than the 3.21-Å value found in methemerythrin. The discrepancy between the X-ray and EXAFS data for deoxy Hr is similar to that found for azidomethemerythrin and is possibly also due to a poor fit of the second shell in the EXAFS data.[29] EXAFS measurements on $[Fe_2(OH)(OAc)_2(Me_3TACN)_2](ClO_4)\cdot H_2O$ may prove helpful in reinterpreting the protein data.

Magnetic Studies. Measurements were carried out on solid samples of **1** and **2** by SQUID susceptometry, and plots for molar susceptibility and effective moment versus temperature are given in Figures 3 and 4. Numerical data are listed in Tables S7 and S8. For both complexes, the temperature-dependent magnetic behavior was modeled by using the theory of Heisenberg, Dirac, and Van Vleck for magnetic coupling in a binuclear system. Neither spin–orbit coupling nor zero-field splitting were modeled in the ferrous complex. The expressions[18] for the temperature-dependent susceptibility may be derived from the general isotropic exchange Hamiltonian, $H = -2J\tilde{S}_1\cdot\tilde{S}_2$, where $S_1 = S_2 = 2$ for **1** and $S_1 = S_2 = {}^5/_2$ for **2**. A Curie-type term was added to correct for a paramagnetic impurity in **1**, while a Curie–Weiss-type term was required in the case of **2**. The resulting expressions for **1** and **2** are given in eq 2 and 3, respectively, where $C = Ng^2\mu_\beta^2/kT$, $x = J/kT$, and p is the mole fraction of a paramagnetic impurity. Optimization of the least-squares fit for **1** gave $g = 2.18$ (1), J = −13.1 (1) cm^{-1}, and $p = 9.9$ (5) × 10^{-3} with a correlation coefficient of 0.9961. The fit is reasonable (Figure 3), even though spin–orbit coupling was neglected. The optimization of the least-squares fit for **2** gave $g = 2.00$ (not varied), $J = -119$ (1) cm^{-1}, $p = 7.3$ (3) × 10^{-3}, and $\theta = -37$ (2) K with a correlation coefficient of 0.9995 (Figure 4). The J value of −119 (1) cm^{-1} obtained for **2** is close to the preliminary value of $J = -115$ cm^{-1} reported earlier for the ClO_4^- salt,[9b] but differs from the −95 (2) cm^{-1} value reported for the PF_6^- salt.[9c] We find no difference in J values for **2** and **3**. A large negative θ value for the paramagnetic impurity was required to obtain good fits in each of four separate studies of compounds **2** and **3**. These results suggest that, perhaps, the impurity is a trinuclear, or other odd-numbered polyiron-containing, antiferromagnetically coupled species.

$$\chi_M = \frac{(1-p)C(2e^{2x} + 10e^{6x} + 28e^{12x} + 60e^{20x})}{1 + 3e^{2x} + 5e^{6x} + 7e^{12x} + 9e^{20x}} + 4.4p/T \quad (2)$$

$$\chi_M = \frac{(1-p)C(2e^{2x} + 10e^{6x} + 28e^{12x} + 60e^{20x} + 110e^{30x})}{1 + 3e^{2x} + 5e^{6x} + 7e^{12x} + 9e^{20x} + 11e^{30x}} + 4.4p/(T-\theta) \quad (3)$$

The −119-cm^{-1} value of J found for **2** implies stronger coupling than that usually observed in simple (μ-oxo)diiron(III) compounds in which values typically lie in the range −80 to −105 cm^{-1},[34,35] but it is comparable to the coupling in other (μ-oxo)bis(μ-carboxylato)diiron(III) compounds, which have J values of −121[8] and −120 cm^{-1}.[21] The antiferromagnetic exchange coupling constants of all of the (μ-oxo)bis(μ-carboxylato)diiron(III) model compounds are thus in reasonably close agreement with the value of $J = -134$ cm^{-1} measured for methemerythrin from *Phascolopsis (syn Goldfingia) gouldii*.[36]

The J value of −13 cm^{-1} measured for $[Fe_2(OH)(OAc)_2(Me_3TACN)_2](ClO_4)$ reveals greatly reduced magnetic coupling compared to the diiron(III) complex and very similar magnetic coupling to that in deoxyhemerythrin, in which J is estimated by MCD–ESR[31b] to be in the range −12 to −38 cm^{-1} and by ^{1}H NMR[10b] to be −15 ± 2 cm^{-1}. Magnetic data for **1** were fit assuming spin–orbit coupling to be negligible, although such may not be the case by analogy to deoxyHr.[31b] By using this same assumption, the J value for deoxyHr was calculated to be in the −20 to −30 cm^{-1} range.[31b] Since no (μ-oxo)- or (μ-aquo)diiron(II) complexes are yet known, the effect of deprotonation or protonation of the μ-hydroxo bridge on the exchange coupling constant is also unknown. By analogy to (μ-oxo)bis(μ-carboxylato)diiron(III) complexes, however, it is likely that protonation of the hydroxo bridge will cause an additional decrease in $|J|$. For example, $[Fe_2O(OAc)_2(HBpz_3)_2]$ has $J = -121$ cm^{-1},[8] while $[Fe_2(OH)(OAc)_2(HBpz_3)_2]^+$ has $J = -17$ cm^{-1}.[20] The similarity in the exchange coupling constants in **1** and deoxyhemerythrin demonstrates that a bridging hydroxo group can adequately account for the magnetic behavior of deoxyhemerythrin. Comparison with carboxylate-bridged compounds[37-39] suggests that these groups will mediate antiferromagnetic coupling of at most −4 cm^{-1}. Taken together, these results argue against the model for deoxy Hr, suggested by EXAFS measurements, in which there is no bridging hydroxo group. It should be noted, however, that azidodeoxyhemerythrin has a paramagnetic ground state[10b,31] in contrast both to deoxyhemerythrin and **1**. This observation is consistent either with hydroxo-bridge cleavage or protonation to form a μ-aqua bridge, induced by the bonding of the azide group.

Mössbauer Spectroscopic Properties. The Mössbauer spectra of $[Fe_2O(OAc)_2(Me_3TACN)_2](PF_6)_2$ and $[Fe_2(OH)(OAc)_2(Me_3TACN)_2](ClO_4)$ were measured at 4.2 and 80 K and in the presence of externally applied magnetic fields parallel to the γ-ray direction. Representative spectra are shown in Figures 5 and 6. In addition, the Mössbauer spectra of $[Fe_2O(OAc)_2(TACN)_2]I_2$[9a] and $[Fe_2(OH)(OAc)_2(HBpz_3)_2](ClO_4)$[20] were measured for comparison. Mössbauer parameters obtained from least-squares fits of the experimental data to Lorentzian line shapes are summarized in Table VI.

(34) Murray, K. S. *Coord. Chem. Rev.* **1974**, *12*, 1–35.
(35) Ou, C. C.; Wollman, R. G.; Hendrickson, D. N.; Potenza, J. A.; Schugar, H. J. *J. Am. Chem. Soc.* **1978**, *100*, 4717–4724.
(36) Dawson, J. W.; Gray, H. B.; Hoenig, H. E.; Rossman, G. R.; Schredder, J. M.; Wang, R.-H. *Biochemistry* **1972**, *11*, 461–465.
(37) Cheng, C.; Reiff, W. M. *Inorg. Chem.* **1977**, *16*, 2097–2103.
(38) Pierce, R. D.; Friedberg, S. A. *Phys. Rev. B: Solid State* **1971**, *3*, 934–942.
(39) Barros, S. d. S.; Friedberg, S. A. *Phys. Rev.* **1966**, *141*, 637–640.

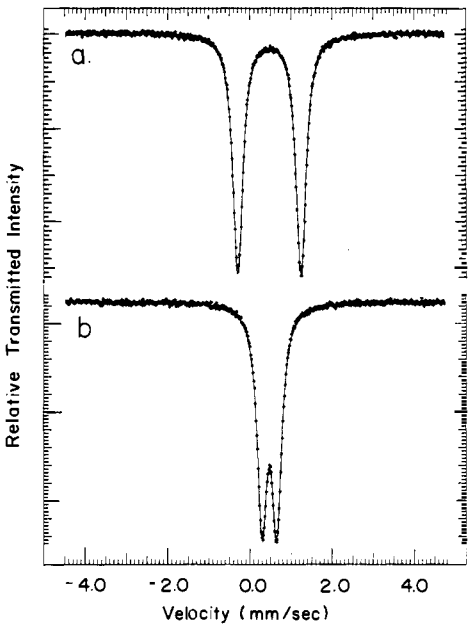

Figure 5. Mössbauer spectrum at 4.2 K of (a) $[Fe_2O(OAc)_2(Me_3TACN)_2](PF_6)_2$ and (b) $[Fe_2(OH)(OAc)_2(HBpz_3)_2](ClO_4)$. The solid line is the theoretical least-squares fit to the experimental data. Mössbauer parameters are given in Table VI.

Table VI. Mössbauer Parameters for Selected Binuclear Iron Model Compounds

complex	temp, K	δ,[a] mm/s	ΔE_Q, mm/s
$[Fe_2O(OAc)_2(Me_3TACN)_2](PF_6)_2$	4.2	0.47 (3)	1.50 (5)
	77	0.47 (3)	1.50 (5)
$[Fe_2(OH)(OAc)_2(Me_3TACN)_2](ClO_4)$	4.2	1.16 (3)	2.83 (5)
	77	1.15 (3)	2.76 (5)
$[Fe_2O(OAc)_2(TACN)_2]I_2$	80	0.46 (3)	1.72 (5)
$[Fe_2(OH)(OAc)_2(HBpz_3)_2](ClO_4)$	80	0.47 (3)	0.25
$[Fe_2O(OAc)_2(HBpz_3)_2]$[b]	4.2	0.52 (3)	1.60

[a] Isomer shifts referenced to metallic iron at room temperature. [b] Reference 8.

The Mössbauer spectrum of $[Fe_2O(OAc)_2(Me_3TACN)_2](PF_6)_2$ at 4.2 and 77 K consists of a symmetric quadrupole doublet with an isomer shift of δ = 0.47 (3) mm/s and a quadrupole splitting of ΔE_Q = 1.50 (5) mm/s. The line widths (full width at half maximum) of Γ = 0.34 mm/s at 4.2 K and Γ = 0.40 mm/s at 77 K are consistent with equivalent iron sites. The isomer shift is well within the range ($0.3 < \delta < 0.6$ mm/s) observed for a wide variety of monomeric and oxo-bridged high-spin ferric complexes.[34,40] The large quadrupole splitting is comparable to that observed both in binuclear 6-coordinate ferric complexes ($\Delta E_Q \sim 1.5$ mm/s)[34,41] and in the met forms of hemerythrin (1.57 mm/s $< \Delta E_Q <$ 2.04 mm/s),[41-44] but it is much larger than the quadrupole splitting observed in mononuclear high-spin ferric complexes ($\Delta E_Q \simeq 0.7$ mm/s).[40] Similar Mössbauer spectral results were obtained for the analogous (μ-oxo)bis(μ-carboxylato) species, $[Fe_2O(OAc)_2(HBpz_3)_2]$ and $[Fe_2O(OAc)_2(TACN)_2]I_2$, with δ = 0.52 (3) mm/s (ΔE_Q = 1.60(5) mm/s)[8] and δ = 0.46 (3) mm/s (ΔE_Q = 1.72 (5) mm/s), respectively. The isomer shifts measured for all of these complexes are the same within experimental error, thus indicating a constant amount of electron density around each iron atom for all cases. The differences observed in the quadrupole coupling constants, however, imply that the electric field gradient does change. The variations observed in the magnitude of the quadrupole coupling constants do not correspond either with changes in the Fe–(μ-oxo) or Fe–(*trans*-N) bond lengths or to small angular distortions from octahedral geometry.

The effect of changes in the electronic symmetry of the iron coordination sphere is nicely illustrated by the results for $[Fe_2(OH)(OAc)_2(HBpz_3)_2](ClO_4)$, which has an extremely small ΔE_Q of 0.3 mm/s, with an isomer shift of 0.47 mm/s. Protonation of the μ-oxo group in $[Fe_2O(OAc)_2(HBpz_3)_2]$ causes a significant alteration in the electronic charge distribution at the iron sites, from a highly asymmetric one in the μ-oxo complex to a more spherically symmetrical one in the μ-hydroxo complex. This electronic charge redistribution is also reflected in the reduction of d-electron orbital overlap, resulting in a diminution of the magnetic exchange coupling constant J from -121 to -17 cm^{-1} upon protonation of the bridging oxygen atom.[20] Concomitantly, the Fe–O bond lengthens from 1.78 to 1.96 Å, and the trans Fe–N bond shortens to the same values observed for the cis Fe–N bond lengths.[20]

The Mössbauer spectrum of $[Fe_2(OH)(OAc)_2(Me_3TACN)_2](ClO_4)$ recorded at 4.2 and 77 K consists of a symmetrical quadrupole doublet. The least-squares fits give an isomer shift of δ = 1.16 (3) mm/s and a quadrupole splitting ΔE_Q = 2.83 (5) mm/s for data at 4.2 K. The observed line widths (Γ = 0.46 mm/s) are somewhat larger than those in the diiron(III) complex. The relatively high value for the isomer shift and the large quadrupole splitting are indicative of high-spin iron(II),[37] consistent with the magnetic results.

The Mössbauer spectra of powdered samples of **1** measured in externally applied fields of 60 and 80 kOe (Figure 6) are consistent with a diamagnetic ground state. A theoretical simulation of the data (Figure 6) gives a positive principal component of the electric field gradient (V_{zz}).

Mössbauer spectra have been recorded for hemerythrin in the oxy, deoxy, and several met forms.[41-44] The spectra of deoxyhemerythrin and most azidomethemerythrin samples show only one type of iron site with typical values of δ = 1.14 mm/s (ΔE_Q = 2.76 mm/s) and δ = 0.45 mm/s (ΔE_Q = 1.76 mm/s), respectively.[43] Oxyhemerythrin Mössbauer spectral results reveal two types of iron atoms in a 1:1 ratio with δ = 0.47 mm/s (ΔE_Q = 1.86 mm/s) and δ = 0.47 mm/s (ΔE_Q = 1.04 mm/s)[43] where, by analogy to the methemerythrin species with N_3O_3 donor sets, the second value appears to correspond to the dioxygen-carrying iron atom with its N_2O_4 donor set. The Mössbauer parameters of **2** (δ = 0.47 mm/s, ΔE_Q = 1.50 mm/s) are similar to those observed for the ferric iron atoms in hemerythrin with N_3O_3 donor sets, the slightly smaller quadrupole coupling constant in the model compound being the most notable difference. Variations in quadrupole coupling constants of this magnitude can be caused by relatively small distortions from octahedral symmetry, as revealed by the crystal structures of **3**, the TACN complex, and the $HBpz_3^-$ complex discussed above, or by changes in the second coordination sphere.

The Mössbauer parameters measured for **1** are identical, within experimental error, with those measured for deoxyhemerythrin. This observation is surprising, since it implies either that both models, the hydroxo-bridged model having one pentacoordinate and one hexacoordinate iron atom and the unbridged model having two pentacoordinate iron atoms, proposed for deoxyhemerythrin are incorrect or that the available Mössbauer spectroscopic results do not distinguish between five- and six-coordinate ferrous atoms in deoxy Hr. The second explanation cannot be dismissed a priori, since the large asymmetry in electron density distribution inherent in a T ground state will minimize the relative distortion in electron distribution caused by changing ligands and will render the quadrupole splitting rather insensitive to the direct ligand contribution to the electric field gradient. Further studies on five- and six-coordinate bridged diiron(II) complexes are necessary to resolve this question.

(40) Gibb, T. C.; Greenwood, N. N. In *Mössbauer Spectroscopy*; Chapman and Hall, Ltd.: London, 1971; pp 148–164.
(41) Okamura, M. Y.; Klotz, I. M.; Johnson, C. E.; Winter, M. R. C.; Williams, R. J. P. *Biochemistry* **1969**, *8*, 1951–1958.
(42) Clark, P. E.; Webb, J. *Biochemistry* **1981**, *20*, 4628–4630.
(43) York, J. L.; Bearden, A. J. *Biochemistry* **1970**, *9*, 4549–4554.
(44) Garbett, K.; Johnson, C. E.; Klotz, I. M.; Okamura, M. Y.; Williams, R. J. P. *Arch. Biochem. Biophys.* **1971**, *142*, 574–583.

Electrochemical Studies. The cyclic voltammetric (CV) results for $[Fe_2O(OAc)_2(Me_3TACN)_2](PF_6)_2$ are displayed in Figure 7. Measurements over the range +1.0 to -1.7 V versus SCE revealed a quasireversible wave at -0.374 V (ΔE_{pp} = 78 mV at a scan speed of 20 mV/s) and an irreversible (reduction only) wave at -1.5 V. Controlled potential coulometry (CPC) experiments at a potential of -0.55 V versus SCE measured 1.03 (10) e^-/mol of **2**, thus supporting an assignment of $Fe_2(III,III) \rightleftharpoons Fe_2(II,III)$ for the quasireversible wave. Cyclic voltammetry experiments carried out on the solution following reduction gave the same voltammogram, confirming that the only electroactive species formed was the putative $Fe_2(II,III)$ complex.

The cyclic voltammogram of $[Fe_2(OH)(OAc)_2(Me_3TACN)_2](ClO_4)$ has one anodic peak at -0.20 V and the return scan shows two peaks at -0.29 and -0.37 V. In order to test the hypothesis that these two peaks resulted from reduction of both oxo- and hydroxo-bridged $Fe_2(II,III)$ species, a small amount of triethylamine (to give a 5 mM solution) was added and the experiment repeated. Since triethylamine is a strong enough base to deprotonate the hydroxo-bridged diiron(III) complex,[20] it is not unreasonable to expect that it can deprotonate a hydroxo-bridged mixed-valence complex. The results showed loss of the reduction wave at -0.29 V, leaving one pseudoreversible wave having $E_{1/2}$ of -0.290 V with a peak-to-peak separation of 130 mV (Figure 7). The reduction peak potential of this wave occurs at -0.36 V, suggesting that the -0.37-V peak in the CV of **1** results from reduction of the oxo-bridged mixed-valence complex. When acetic acid was added instead of triethylamine to give a 7-mmol solution, the electrochemistry became completely irreversible, resulting in an oxidation peak at +0.07 V with a corresponding reduction peak at -0.32 V (data not shown). The peaks observed in the neutral solution thus appear to correspond to oxidation of the hydroxo-bridged diiron(II) complex to a mixture of oxo- and hydroxo-bridged mixed-valence diiron(II,III) species.

Controlled-potential coulometry experiments on **1** at -0.14 V in the presence of triethylamine give 1.83 (20) e^-/Fe_2 unit. Since -0.14 V is more positive than the potential of -0.374 V measured for the $Fe_2(III,III) \rightleftharpoons Fe_2(II,III)$ couple, the CPC results cannot distinguish between a "2-electron" process and two "1-electron" processes in which the mixed-valence species forms and is further oxidized during the CPC experiment. In other words, it is possible that the CV study of **1** measures the $Fe_2(III,II) \rightleftharpoons Fe_2(II,II)$ wave, while under the exhaustive conditions of the CPC experiment, the material oxidizes completely to $Fe_2(III,III)$. This latter interpretation is supported by the observation that a cyclic voltammogram of a mixture of **1** and **2** appears to be a superposition of the CV's of pure **1** and **2**, implying that the observed waves for **1** do not correspond to the $Fe_2(III,III) \rightleftharpoons Fe_2(II,II)$ couple. The observation for **1** that it is easier to stop at the mixed-valence oxidation state when reducing the diiron(III) complex than when oxidizing the diiron(II) complex in the CPC experiments parallels the behavior of the protein and may be due to the necessity of providing protons to form hydroxo- or aquo-bridged $Fe_2(II,II)$ species. In hemerythrin, $(semi\text{-}met)_R$ is easier to produce than $(semi\text{-}met)_O$, since many reductants will add only one electron to Hr but it is difficult to remove only one electron from deoxyHr, the second electron being transferred more quickly than the first with most oxidants.[45,46]

The electrochemical results thus suggest that a mixed-valence species is produced in solution from the diiron(III) and, less definitively, diiron(II) complexes. These results also reveal that the mixed-valence species is unstable with respect to disproportionation, since in the presence of base the oxidation of the ferrous complex is at least 85 mV more positive than the reduction of the ferric compound in methylene chloride solution. Attempts to stabilize the mixed-valence oxidation state by changing the solvent to water, methanol, acetonitrile, or solvent mixtures were unsuccessful. The instability of the mixed-valence oxidation state parallels that of the mixed-valence forms of hemerythrin, which are also unstable with respect to disproportionation;[46,47] deoxyhemerythrin is oxidized to the $(semi\text{-}met)_O$ form at 0.06 V versus SCE and methemerythrin is reduced to $(semi\text{-}met)_R$ at -0.13 V versus SCE.[48] The disproportionation reaction of semimethemerythrin has been found to be a first-order process[45,47] with sufficiently rapid rates to suggest iron valence delocalization.[45] Although semimethemerythrin is thermodynamically unstable, the long distance between the binuclear iron centers (28 to 30 Å) slows the disproportionation reaction sufficiently to allow isolation and study of the semimet species.[45-47] Despite the large separation between the iron centers, the disproportionation reactions for many types of semimethemerythrin are complete within 30 min.

Properties of the Mixed-Valence $Fe_2(II,III)$ Complex. Controlled-potential electrolysis of $[Fe_2O(OAc)_2(Me_3TACN)_2](PF_6)_2$ at -0.55 V versus SCE for several hours gave a deep green solution which took up a total of 1 equiv of electrons per binuclear iron complex. Electron spin resonance studies on this reaction mixture (Figure 8) support the existence of the binuclear mixed-valence species, since g values less than 2, which are extremely rare for iron,[49-52] are found in mixed-valence species. The observed ESR spectrum contains features similar to those reported for azidosemimethemerythrin (g values of 1.93, 1.72, and 1.57)[53,54] and to those observed for the mixed-valence binuclear iron center in the enzymes purple acid phosphatase (g values of 1.93, 1.72, and 1.56)[55] and methane monooxygenase (g values of 1.95, 1.88, and 1.78).[4] The major differences in the ESR spectra are the much larger line widths and the addition of a feature at $g \sim 1.6$ in semimethemerythrin and purple acid phosphatase. Double integration of the ESR spectrum with copper(II) sulfate as a standard indicated that the signal corresponds to 65% of the intensity expected for one additional electron per diiron unit, thus revealing the mixed-valence species to be relatively stable in dilute solution.

Mössbauer experiments performed on the solid material remaining after removal of the solvent in vacuo gave inconsistent results. Although several samples had Mössbauer spectra that appeared to be superpositions of approximately equal quantities of **1** and **2**, as expected for a mixed-valence complex, others contained a quadrupole doublet resulting either from **1** or from **2** along with other broad, unassignable peaks. Magnetic Mössbauer experiments, performed on a sample with a "good" zero field Mössbauer spectrum, showed the presence of 10–20% paramagnetic Fe^{3+} and Fe^{2+} ions with reduced hyperfine fields of -230 and +103 kOe, respectively. This result is consistent with a binuclear complex of high-spin Fe^{3+} and Fe^{2+} with a ground-state spin $S = {}^1/_2$,[56] suggesting the presence of a mixed-valence species.

(45) Harrington, P. C.; Wilkins, R. G. *J. Am. Chem. Soc.* **1981**, *103*, 1550–1556.

(46) Nocek, J. M.; Kurtz, D. M., Jr.; Pickering, R. A.; Doyle, M. P. *J. Biol. Chem.* **1984**, *259*, 12334–12338.

(47) Babcock, L. M.; Bradic, Z.; Harrington, P. C.; Wilkins, R. G.; Yoneda, G. S. *J. Am. Chem. Soc.* **1980**, *102*, 2849–2850.

(48) Armstrong, F. A.; Harrington, P. C.; Wilkins, R. G. *J. Inorg. Biochem.* **1983**, *18*, 83–91.

(49) Loew, G. H. *Biophys. J.* **1970**, *10*, 196–212.

(50) Blumberg, W. E.; Peisach, J. In *Probes of Structure and Function of Macromolecules and Membranes, Proceedings of the Colloquim of the Johnson Research Foundation, 5th*; Chance, B., Ed.; Academic: New York, 1969 (Pub. 1971); Vol. 2, pp 215–229.

(51) Low, W. *Solid State Phys. Suppl.* **1960**, *2*, 76–113.

(52) Palmer, G.; Brintzinger, H.; Estabrook, R. W.; Sands, R. H. In *Magnetic Resonance in Biological Systems*; Ehrenberg, A., Malmström, B., Vänngård, T., Eds.; Pergamon Press: New York, 1967; pp 159–171.

(53) Martinsen, J.; Irwin, M. J.; Ho, P. S.; Hoffman, B. M.; Klotz, I. M. *Biochem. Biophys. Res. Commun.* **1983**, *112*, 954–956.

(54) Muhoberac, B. B.; Wharton, D. C.; Babcock, L. M.; Harrington, P. C.; Wilkins, R. G. *Biochim. Biophys. Acta* **1980**, *626*, 337–345.

(55) Debrunner, P. G.; Hendrich, M. P.; DeJersey, J.; Keough, D. T.; Sage, J. T.; Zerner, B. *Biochim. Biophys. Acta* **1983**, *745*, 103–106.

(56) Cammack, R.; Dickson, D. P. E.; Johnson, C. E. In *Iron Sulfur Proteins*; Lovenberg, W., Ed.; Academic: New York, 1977; Vol. III, p 305.

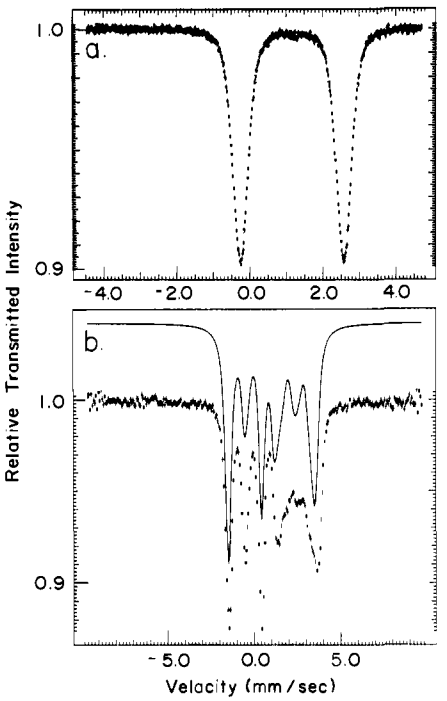

Figure 6. Mössbauer spectrum of $[Fe_2(OH)(OAc)_2(Me_3TACN)_2](ClO_4)$ at 4.2 K (a) in the absence of an applied magnetic field and (b) at T = 4.2 K and H_0 = 80 kOe parallel to the γ-ray direction. The solid line gives a theoretical simulation of (b) with δ = 1.16 mm/s, ΔE_Q = 2.83 mm/s, and H_0 = 80 kOe.

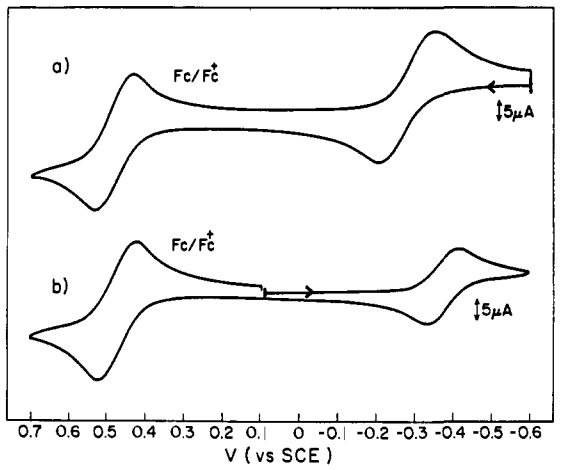

Figure 7. Cyclic voltammogram of (a) **1** with 5 mM triethylamine and (b) **2** at 50 mV/s scan speeds in methylene chloride containing 0.2 M tetra-*n*-butylammonium perchlorate. Voltage readings are referenced to the saturated calomel electrode. Ferrocene was added as an internal calibrant.

Firm identification of such a complex was hindered, however, by the presence of large amounts of diamagnetic Fe^{3+} and Fe^{2+} species. These Mössbauer results are probably a function of sample preparation, the disproportionation reaction being facilitated by concentration of the sample to dryness.

Attempts to synthesize the mixed-valence complex by chemical oxidation of **1** were unsuccessful. Reactions of **1** with 1 equiv of silver nitrate, silver acetate, iodine, or ferricinium hexafluorophosphate in either methanol, methylene chloride, or acetone resulted in solutions that contained **2**, presumably with equal amounts of **1**, judging by UV–vis spectroscopy. In contrast, reduction of **2** with cobaltocene in methylene chloride (one electron reductant, E_f = –0.78 V) gave a solution that had a pseudoreversible oxidation wave at –0.37 V, thus implying the formation of the mixed-valence complex. ESR spectroscopy on the same sample showed a broad peak with g = 1.92, thus supporting the presence of a mixed-valence species. Mössbauer results were inconclusive, and attempts to isolate the mixed-valence complex by this route were unsuccessful.

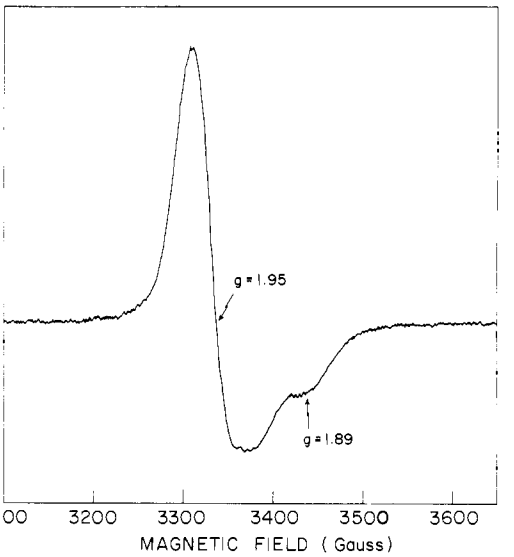

Figure 8. ESR spectrum of the mixed-valence diiron(II,III) complex at 9.6 K in a 1:1 acetonitrile:toluene glass with microwave frequency of 9.0919 GHz, microwave power of 0.2 mW, modulation amplitude of 0.5 G, modulation frequency of 100 KHz, and time constant of 0.3 s. Features marked by "g values" are for identification purposes only and were not taken from any theoretical fit of the data.

Conclusions

The first pair of model compounds for the two biologically relevant redox states of hemerythrin, methemerythrin and deoxyhemerythrin, have been synthesized and their redox chemistry has been studied.

The binuclear ferric complex **2**, which is very similar to several previously reported complexes,[8,9a,22] mimics the structural and physical characteristics of azidomethemerythrin quite well. Comparison of the Mössbauer spectra and crystal structures of **2**, $[Fe_2O(OAc)_2(HBpz_3)_2]$,[8] and $[Fe_2O(OAc)_2(TACN)_2]I_2$[9a,22] demonstrates that relatively small distortions in the coordination geometry, or changes in the second coordination sphere, around the iron atoms are needed to achieve the somewhat higher quadrupole coupling constants observed in the protein.

The properties of the binuclear ferrous complex **1** strongly support the model proposed for deoxyhemerythrin on the basis of X-ray diffraction, NMR, and MCD–ESR measurements. The observed iron–iron distance and the temperature-dependent magnetic behavior provide support for the postulated presence of the bridging hydroxo group in the protein, while the available Mössbauer studies are unable to distinguish either the bridged or unbridged hydroxo group models.

The electrochemical behavior of both **1** and **2** mimics the redox behavior of hemerythrin quite successfully. As with hemerythrin, reduction of **2** occurs at a lower potential than oxidation of **1**, forming a mixed-valence species that is unstable with respect to disproportionation in the presence of protons. Electron spin resonance spectral features at $g < 2.0$ and reduced hyperfine fields in the magnetic Mössbauer spectrum of species generated from $[Fe_2O(OAc)_2(Me_3TACN)_2]^{2+}$ are consistent with a mixed-valence diiron(II,III) formulation. Two related, mixed-valence diiron(II,III) complexes having phenoxo bridges are also known.[57]

Acknowledgment. This work was supported by U.S. Public Health Service Grant GM 32134 (to S.J.L.) from the National Institute of General Medical Sciences. J.R.H. was a recipient of a National Research Service Award (GM 10808) from the NIGMS. The Francis Bitter National Magnet Laboratory is supported by the National Science Foundation. We thank Dr.

(57) (a) Suzuki, M.; Uehara, A.; Endo, K. *Inorg. Chim. Acta* **1986**, *123*, L9–L10. (b) Murch, B. P.; Borovik, A. S.; Papaefthymiou, V.; Que, L., Jr. *Recl. Trav. Chim. Pays-Bas* **1987**, *106*, 247.

S. M. Gorun for helpful comments.

Registry No. 1, 98839-70-4; 2, 96556-04-6; 3, 110827-36-6; $Fe(Me_3TACN)Cl_3$, 110827-37-7; $[Fe_2O(OAc)_2(TACN)_2]I_2$, 110827-38-8; $[Fe_2(OH)(OAc)_2(HBpz_3)_2](ClO_4)$, 90886-31-0; $[Fe_2O(OAc)_2(Me_3TACN)_2]^+$, 110827-39-9; $[Fe_2(OH)(O_2CCH_3)_2(Me_3TACN)_2]^{2+}$, 110851-24-6.

Supplementary Material Available: Tables reporting thermal parameters for all atoms and fixed hydrogen atom positional parameters and χ_{obsd}, χ_{calcd}, μ_{obsd}, and μ_{calcd} for **1** and **2** (6 pages); listing of observed and calculated structure factor amplitudes (23 pages). Ordering information is given on any current masthead page.

Syntheses of η^5-Heterocyclic Manganese Tricarbonyls. Effect of the Heteroatom and Heterocycle Ring Substituents on CO Substitution Reactions

David L. Kershner and Fred Basolo*

Contribution from the Department of Chemistry, Northwestern University, Evanston, Illinois 60201. *Received April 7, 1987*

Abstract: The syntheses and characterizations of some new η^5-heterocyclic manganese tricarbonyl complexes are described. Kinetic studies are reported for CO substitution reactions of these nitrogen family η^5-dimethylheterocyclic manganese tricarbonyl complexes. The results show that only the *N*-heterocycle compounds undergo CO substitution by phosphorus nucleophiles. These results are attributed to the greater electronegativity of N than that of C, P, or As. Both tricarbonyl(η^5-3,4-dimethylpyrrolyl)manganese(I) and tricarbonyl(η^5-2,5-dimethylpyrrolyl)manganese(I) substitute CO by an associative pathway in which the reaction rates are first order in concentration of metal complex and first order in concentration of entering nucleophile. The former compound also substitutes CO by a pathway that is independent of the concentration of incoming nucleophile. The second-order pathway is believed to involve a ring-slippage ($\eta^5 \rightarrow \eta^3 \rightarrow \eta^5$) mechanism, whereas the first-order pathway appears to involve a ligand-dissociation mechanism.

The kinetics and mechanisms of carbon monoxide substitution reactions of η^5-cyclopentadienyl[1] and of η^5-indenyl[2] metal carbonyl complexes have received much attention. The reactions take place by an associative process, which is presumed to involve the intermediate formation of an η^3 bound π-cyclic group upon attack at the metal center by an incoming nucleophile (eq 1). This η^5

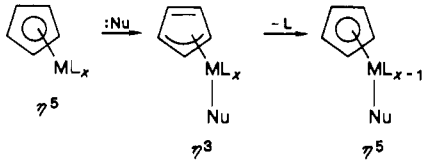

(1)

$\rightarrow \eta^3 \rightarrow \eta^5$ ring slippage maintains an 18-electron count of the metal center and thereby avoids the energetically unfavorable 20-electron transition state that would result if a pair of electrons on the metal were not localized on a ligand.[1d,3]

In recent papers we have reported[4] and reviewed[5] the syntheses and CO substitution reactivity of η^5-heterocyclic metal carbonyl complexes. These compounds have been studied much less than have their η^5-carbocyclic analogues,[6] and several of the compounds investigated here had to be prepared and characterized for the first time. Most of the work in this area has involved the synthesis of tricarbonyl(η^5-pyrrolyl)manganese(I)[7] (I) and of its P analogue

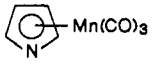

I

tricarbonyl(η^5-phospholyl)manganese(I).[8] Reactivity studies on these compounds have largely been limited to aromatic substitution reactions on the η^5-heterocyclic ring. Our earlier studies of CO substitution reactions of these compounds dealt with the N analogues of tricarbonyl(η^5-cyclopentadienyl)manganese(I) and of tricarbonyl(η^5-indenyl)manganese(I).

These η^5-heterocycle metal carbonyls were found[4b] to undergo associative CO substitution reactions at a much faster rate than their η^5-carbocyclic counterparts. For example, I was found to readily substitute CO at elevated temperatures with phosphorus nucleophiles, in contrast to the reported[9] inertness of the C analogue tricarbonyl(η^5-cyclopentadienyl)manganese(I). It was suggested[4b] that this enhanced reactivity may be due to the greater efficiency of the more electronegative N in removing electron density from the metal center. Such electron delocalization to the cyclic ligand is required by the proposed $\eta^5 \rightarrow \eta^3 \rightarrow \eta^5$

(1) (a) Kowaleski, R. M.; Trogler, W. C.; Basolo, F. *Gazz. Chim. Ital.* **1986**, *116*, 105-107. Kowaleski, R. M.; Basolo, F.; Trogler, W. C.; Ernst, R. D. *J. Am. Chem. Soc.* **1986**, *108*, 6046-6048. (b) Palmer, G. T.; Basolo, F.; Kool, L. B.; Rausch, M. D. *J. Am. Chem. Soc.* **1986**, *108*, 4417-4422. (c) Rerek, M. E.; Basolo, F. *J. Am. Chem. Soc.* **1984**, *106*, 5908-5912. (d) Schuster-Woldan, H. G.; Basolo, F. *J. Am. Chem. Soc.* **1966**, *88*, 1657-1163.

(2) (a) Liang-Nian, J.; Rerek, M. E.; Basolo, F. *Organometallics* **1984**, *3*, 740-745. (b) Rerek, M. E.; Liang-Nian, J.; Basolo, F. *J. Chem. Soc., Chem. Commun.* **1983**, 1208-1209.

(3) Basolo, F. *Inorg. Chim. Acta* **1985**, *100*, 33-39, and references therein.

(4) (a) Kershner, D. L.; Rheingold, A.; Basolo, F., *Organometallics* **1987**, *6*, 197-198. (b) Liang-Nian, J.; Kershner, D.; Rerek, M. E.; Basolo, F. *J. Organomet. Chem.* **1985**, *296*, 83-94.

(5) Kershner, D. L.; Basolo, F. *Coord. Chem. Rev.* **1987**, *79*, 279-292.

(6) For an extensive review of π-heterocyclic metal complexes see: Novi, M.; Giuseppe, G.; Dell'Erba, C. *J. Heterocycl. Chem.* **1975**, *12*, 1055-1081.

(7) (a) Kursanov, D. N.; Setkina, V. N.; Pyshnograeva, N. I. *Bull. Acad. Sci. USSR, Div. Chem. Sci. (Engl. Transl.)* **1984**, *33*, 807-812. (b) King, R. B.; Efraty, A. *J. Organomet. Chem.* **1969**, *20*, 264-268. (c) Joshi, K. K.; Pauson, P. L.; Qazi, A. R.; Stubbs, W. H. *J. Organomet. Chem.* **1964**, *1*, 471-475.

(8) (a) Mathey, F.; Mitschler, A.; Weiss, r. *J. Am. Chem. Soc.* **1978**, *100*, 5748-5755. (b) Mathey, F. *Tetrahedron. Lett.* **1976**, *46*, 4155-4158. (c) Breque, A.; Mathey, F. *J. Organomet. Chem.* **1978**, *144*, C9-C11. (d) Mathey, F. *J. Organomet. Chem.* **1975**, *93*, 377-388.

(9) Angelici, R. S.; Lowen, W. *Inorg. Chem.* **1967**, *6*, 682-686.

0002-7863/87/1509-7396$01.50/0